Diamagnetic shifts of subbands and the quantum Hall effect of silicon delta -doped $Ga_{0.47}In_{0.53}As$ layers

1993 J. Phys.: Condens. Matter 5 1091

(http://iopscience.iop.org/0953-8984/5/8/010)

J. Phys.: Condens. Matter 5 (1993) 1091–1098. Printed in the UK

Diamagnetic shifts of subbands and the quantum Hall effect of silicon δ-doped $Ga_{0.47}In_{0.53}As$ layers

G Nachtwei, S Heide, H Künzel† and W Passenberg†

Humboldt-Universität zu Berlin, Institut für Festkörperphysik, Invalidenstraße 110, D-O-1040 Berlin, Federal Republic of Germany

† Heinrich-Hertz-Institut für Nachrichtentechnik GmbH, Einsteinufer 37, D-W-1000 Berlin 10, Federal Republic of Germany

Received 7 September 1992, in final form 2 November 1992

Abstract. Magnetotransport investigations of silicon δ-doped $Ga_{0.47}In_{0.53}As$ layers with different electron densities were performed in tilted magnetic fields up to 12 T. The conduction electrons of the samples showed two-dimensional behaviour determined by the dependence of the Hall coefficient on the tilt angle of the magnetic field. Several populated subbands were identified by the normal and the diamagnetic Shubnikov–de Haas effect. The diamagnetic depopulation features of the samples were explained on the basis of calculations done by Reisinger and Koch for symmetrical potential wells. Whereas no quantum Hall effect could be observed at any of the samples in perpendicular magnetic fields up to 12 T, well developed quantum Hall plateaux occurred at a sample with a low doping level above a certain tilt angle. This was found to be due to the depopulation of the higher subbands by the parallel component of the magnetic field.

1. Introduction

The development of new crystal growth techniques such as metalorganic chemical vapour deposition (MOCVD) and molecular beam epitaxy (MBE) facilitated the possibility of growing semiconductor devices with sheet doping of a few or even one single atomic layer (δ-doping layers) [1]. These δ-doping layers are interesting both for fundamental studies of two-dimensional carrier systems [2] and for device applications [3]. In particular access to high electron densities (above $n_s = 10^{13}$ cm^{-2}) and simultaneously rather high electron mobilities provide the possibility of the development of fast and current-stable devices like MESFETs on the basis of δ-doping layers [3].

Research has been focused mainly on Si-doping layers in GaAs up to now [4–6]. However, increasing attention is being paid to silicon δ-doping layers with $Ga_{0.47}In_{0.53}As$ (lattice-matched on InP) as host material [7, 8].

In this paper, we report on the growth and characterization of silicon δ-doped $Ga_{0.47}In_{0.53}As$ layers. The samples were grown by MBE [9]. The sheet resistance and the Hall effect were measured to evaluate the mobile electron density and the Hall mobility. Shubnikov–de Haas (SdH) measurements were performed to determine the population of the electric subbands in the potential well of the samples.

The two-dimensional behaviour of the electron system adjacent to the δ-doping layer was tested by tilting the samples with respect to the direction of the magnetic field. The sample with a low dopant density bore well developed quantum Hall

0953-8984/93/081091+08$07.50

(QH) plateaux in the presence of a parallel magnetic field component sufficiently high to reduce the number of populated subbands. The depopulation of the different subbands in parallel magnetic fields was studied by means of the diamagnetic SdH effect (DSdH) and explained within the model of Reisinger and Koch [10].

2. Sample characteristics and experimental set-up

The $Ga_{0.47}In_{0.53}As$ layers were grown onto (100)-oriented InP:Fe substrates using elemental source MBE. The slightly As-stabilized growth was performed under constant growth conditions of a V/III beam-equivalent pressure ratio kept at 15, a growth temperature of 500 °C, and a growth rate of approximately 1 μm h^{-1}. Silicon was applied as the n-type dopant. A constant Si-cell temperature of 1080 °C was maintained throughout this study, delivering a doping level of 2.5×10^{18} cm^{-3} in homogeneously doped layers. The variation of the areal doping concentration in the δ-doped samples was achieved by different growth interruption times between 5 and 300 s for the deposition of the silicon atoms. The confinement of the silicon doping layer was tested by secondary ion mass spectroscopy (SIMS). Up to areal doping levels of 1×10^{13} cm^{-2}, the doping layer extent in the growth direction is below the sensitivity limit of the SIMS facility of about 7 nm. The silicon δ-doping plane was clad between 0.5 μm thick undoped $Ga_{0.47}In_{0.53}As$ layers. The unintentional background doping of these layers is below the level of 2×10^{15} cm^{-3} and due to residual silicon of the In source.

Three silicon δ-doped samples with different areal dopant densities, $N_D^{(2D)}$, are the subject of this study. The samples were cut into pieces of approximately 3×3 mm^2 and contacted by soldering copper wires with In to the sample surface in the van der Pauw configuration. The electron density, n_s, and the Hall mobility, μ_H, were evaluated at room temperature, $T = 77$ K and $T = 1.3$ K. The subband populations, n_{si}, were determined by SdH experiments with the magnetic field perpendicular to the sample surface.

All magnetotransport investigations were performed using a 13 T superconducting magnet system with an inner cryostat separating the sample thermally from the helium bath of the solenoid. Temperatures down to $T = 1.3$ K were maintained by pumping the He^4 bath of the inner cryostat. The measurements were done using DC currents ($1\ \mu A \leqslant I \leqslant 50\ \mu A$) supplied by a ground-free commercial current source. The data were taken by a high-resolution digital data processing system including two $6\frac{1}{2}$-digit precision voltmeters. This technique allowed us to differentiate the SdH spectra and to detect even weak oscillations at lower magnetic fields.

The samples were mounted onto a sample holder capable of *in situ* rotation with respect to the magnetic field direction in the angular range of $-105° \leqslant \Phi \leqslant 105°$ (Φ is the angle between the normal vector of the sample plane and the magnetic field direction).

3. Experimental results

The expected free-carrier densities and the results of the Hall and SdH measurements of the three samples investigated are summarized in table 1.

The expected carrier densities, $N_D^{(2D)}$, were calculated using the deposition times of 5 s, 50 s, and 80 s for the increasing carrier concentrations, respectively, together

Table 1.

Sample	$N_D^{(2D)}$ (10^{12} cm^{-2})	n_s (10^{12} cm^{-2})	μ_H (cm^2 V^{-1} s^{-1})	i	n_{si} (10^{11} cm^{-2})
sδ-2364	0.63	0.82	5800	0	6.9
				1	1.5
sδ-2329	6.25	6.0	5030	0	$\leqslant$ 49.3[a]
				1	9.0
				2	1.7
sδ-2330	10.00	9.3	3780	0	$\leqslant$ 77.5[a]
				1	13.0
				2	2.2

[a] Estimated from the difference between the Hall and SdH data, not detectable in the SdH signal up to $B = 12$ T.

with reference data. The measured and expected concentrations coincide to within 10% for high doping levels. For the sample with the low δ-doping level, the measured value is higher. This is attributed to an uncertainty in the deposition time, because the time for opening and closing the shutters is approximately 1 s. The influence of parallel conduction due to residual carrier concentration in the cladding layers cannot account for the difference in the measured and the expected carrier density values as the Hall and the SdH data coincide within experimental error at $T = 1.3$ K.

Figure 1 shows the SdH and Hall trace for sample sδ-2329 at $T = 1.3$ K up to $B = 12$ T. The slope of the Hall trace yields the overall electron concentration, n_s, whereas the analysis of the different periods observable in the SdH trace yields the subband populations, n_{si}. The Hall resistance ρ_{xy} and the magnetoresistance R_{xx} of the samples were measured at different angles Φ. To calibrate the rotation gear and to check the two-dimensional behaviour of the samples, the SdH signal was taken while rotating the sample in a fixed magnetic field ($B_0 = 11.56$ T). The positions of the magnetic field parallel to the sample plane are then characterized by well defined R_{xx} minima, if the sample has a positive magnetoresistance [11].

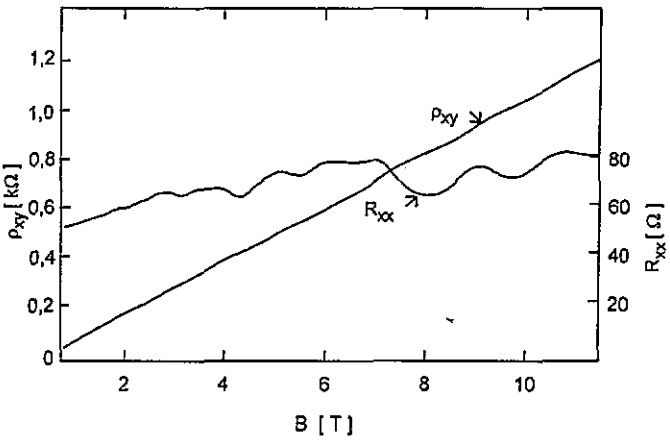

Figure 1. Magnetoresistance R_{xx} and Hall resistance ρ_{xy} of sample sδ-2329 versus magnetic field ($T = 1.3$ K).

Figure 2 presents the Hall resistance of sample sδ-2329 at different fixed angles Φ. Since the Hall coefficient $R_H^{(2D)}$ is dependent only on the magnetic field component $B_\perp$ perpendicular to the two-dimensional electron system (2DES):

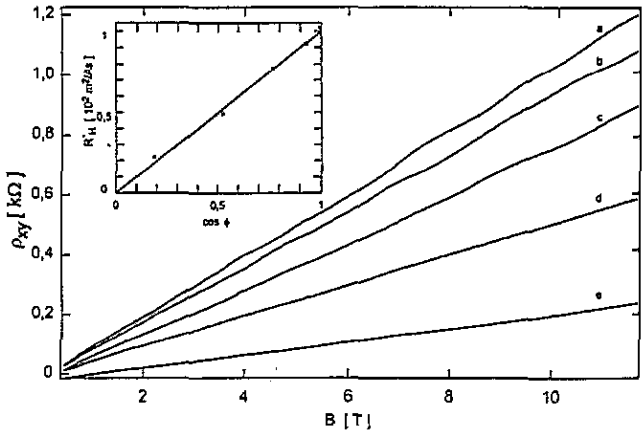

Figure 2. Hall resistance of sample sδ-2329 versus magnetic field at different tilt angles Φ ($T = 1.3$ K), curve a: $\Phi = 0°$, b: 20°, c: 40°, d: 60°, e: 80°. The inset shows the linear relation between the slope of the Hall traces R_H^* and $\cos\Phi$.

$$R_H^{2D} = 1/en_s = U_H/IB_\perp \tag{1}$$

$$B_\perp = B\cos\Phi \tag{1a}$$

where U_H is the Hall voltage and e the electron charge; the slope of the Hall trace $R_H^*(\Phi) = \Delta\rho_{xy}/\Delta B$ is proportional to $\cos\Phi$. This is visible in the inset of figure 2 and proves the 2D behaviour of sample sδ-2329.

Figure 3 shows the Hall traces for the sample sδ-2364 with the lower doping density N_D and a rather small n_s. At lower fields, the Hall traces are linear and behave qualitatively as those of the highly doped sample sδ-2329. Furthermore, for tilt angles $\Phi \geqslant 30°$ well pronounced QH plateaux appear for filling factors (quantum numbers) $j = 4$ and $j = 3$. No QH plateaux are visible for $\Phi = 0°$ (B perpendicular to the layer) up to 12 T. Simultaneously, the magnetoresistance is non-zero in the entire magnetic-field range (figure 4, curve (a)). Figure 4 shows the SdH traces for the same angles Φ as in figure 2. In accordance to the development of the QH plateaux with increasing tilt angle, the corresponding R_{xx} minimum values for the filling factors $j = 4$ and $j = 3$ decrease. The finite resistance R_{xx} in the QH plateau region indicates either some remaining parallel conduction via the $Ga_{0.47}In_{0.53}As$ layers too small to be detected by comparison of the Hall and the SdH results (see table 1), or a finite density of states (DOS) of mobile electrons at the Fermi energy due to a considerable broadening of the Landau levels (referring to the sample mobility which indicates a rather high scattering rate of 7.2×10^{12} s^{-1}).

In principle, the finite longitudinal resistance also modifies the Hall traces due to the van der Pauw geometry of the samples used in this study. If the contacts used as potential probes are not located exactly opposite one another with respect to the current flow direction, a correction term proportional to ρ_{xx} has to be taken into account. However, these modifications become minimal just within the QH plateau. Hence, these modifications are only relevant for filling factors between the plateaux. To avoid the Corbino effect, the contacts were placed in the sample corners touching the sample edges.

Thus, the higher the parallel component of the magnetic field at a certain integer filling factor, the more pronounced the QHE will be.

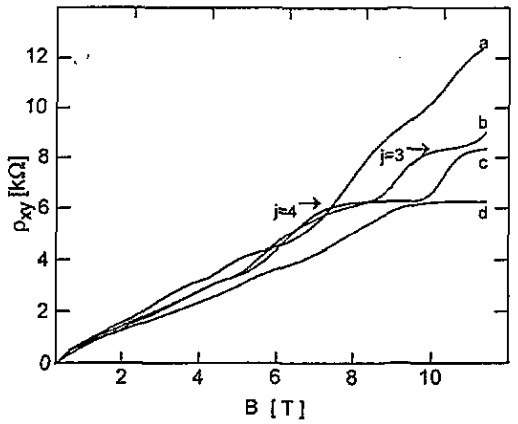

Figure 3. Hall resistance of sample sδ-2364 versus magnetic field at different tilt angles Φ ($T = 1.3$ K), curve a: $\Phi = 0°$, b: 20°, c: 30°, d: 45°. The Hall plateaux $j = 3$ and $j = 4$ are visible in curves b–d.

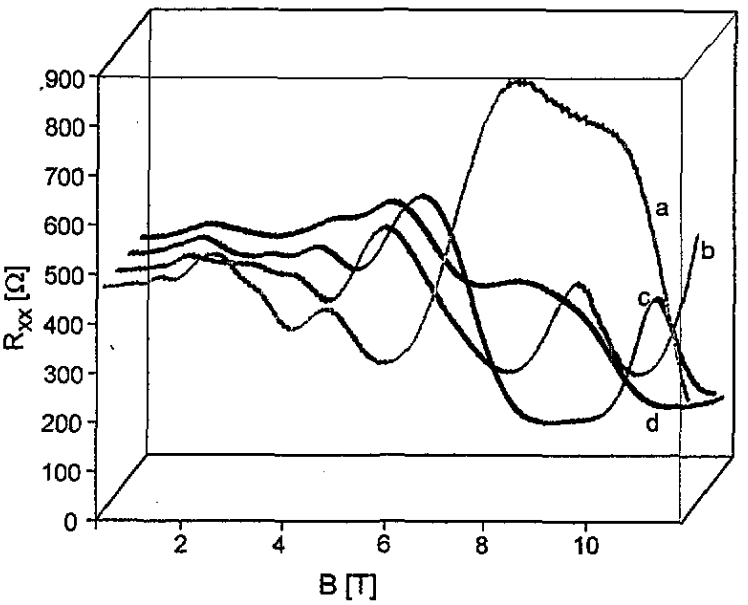

Figure 4. Magnetoresistance R_{xx} of sample sδ-2364 versus magnetic field at different tilt angles Φ (angles as in figure 3, $T = 1.3$ K).

We found the same tendency for rotating the sample in a fixed magnetic field of $B = 11.56$ T. We measured the Hall resistance ρ_{xy} and the SdH resistance of the sample sδ-2364 as functions of the tilt angle Φ. In figure 5, the QH plateaux $j = 2$, 3 and 4 are visible. The deepest minimum of the corresponding $R_{xx}(\Phi)$ trace occurs for the plateau $j = 4$ at $\Phi = 48.8°$, $B_{\parallel} = 8.69$ T and $B_{\perp} = 7.62$ T. At this parallel field, all upper subbands are completely emptied. This is the condition to provide a gap between two quantum levels at the Fermi energy which is not reduced by an interfering level of a higher subband (see e.g. [12]). At a tilt angle of $\Phi = 0°$ (without

a parallel magnetic field), the magnetic field has to be high enough to realize the population of the lowest quantum levels of the $i = 0$ subband only or at least to provide a gap between neighbouring quantum levels (originating from any subband) large enough to keep the adjacent mobility edges apart. In our case, this is valid for magnetic fields $B \geqslant 11.5$ T ($\Phi = 0°$) where the $j = 2$ plateau begins to develop (figure 3, curve (a)).

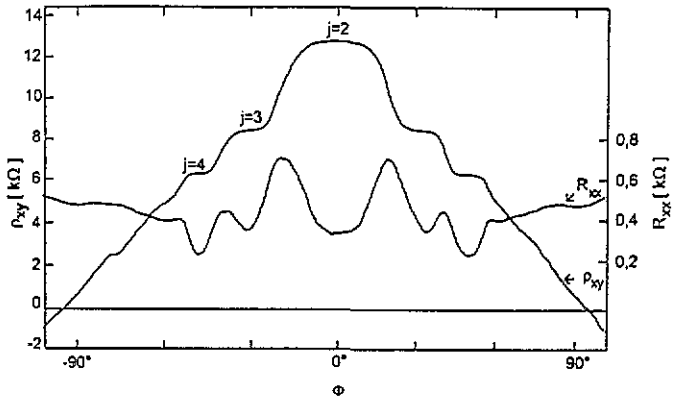

Figure 5. Magnetoresistance R_{xx} and Hall resistance ρ_{xy} of sample sδ-2364 versus tilt angle Φ at a fixed magnetic field of $B = 11.56$ T ($T = 1.3$ K). The QH plateaux $j = 2$, 3 and 4 are well observable in this plot.

The depopulation of the higher subbands by parallel magnetic fields can be observed in the DSdH effect. As is visible in figure 6(a), the diamagnetic depopulations of the subbands $i = 2$ and $i = 1$ occur at $B_{\|} = 1.7$ T and 5.6 T, respectively. The plateaux $j = 3$ and $j = 4$ of the Hall curve at $\Phi = 20°$ (figure 3(b)) correspond to parallel magnetic field components of $B_{\|} = 3.45$ T and 2.56 T, respectively. Hence, these plateaux are realized by quantum levels of the $i = 0$ and $i = 1$ subbands. The same is valid for the $i = 4$ plateau of the Hall curve at $\Phi = 30°$ (figure 3(c)) corresponding to a parallel magnetic field of $B_{\|} = 4.25$ T. Only levels from the ground subband contribute to the $j = 3$ plateau at this angle ($B_{\|} = 5.75$ T). The $j = 4$ plateau at $\Phi = 45°$ occurs at a parallel component of $B_{\|} = 7.8$ T. Hence, the $i = 1$ subband is completely emptied and the QH plateau is as well developed as the $j = 3$ plateau at $\Phi = 30°$. The DSdH effect results of the higher doped samples sδ-2329 and sδ-2330 are presented in figure 6(b) and (c). The subsequent depopulation of the subbands $i = 5$, 4 and 3 are clearly visible in the magnetic field range up to 12 T. Hence, much higher magnetic fields would be required at any tilt angle to observe the QHE at these samples.

The depopulation fields of the device sδ-2364, sδ-2329 and sδ-2330 agree well with the predictions of the model of Reisinger and Koch [10] for symmetrical potential wells. These calculations were done for doping layers with δ-like confinement. The real distribution of the dopants over a finite extent in growth direction results in a round shape of the bottom of the potential well instead of the sharp edge derived from the model [13]. However, the extent of the dopant distribution of our samples is low in comparison to the entire extent of the conducting sheet (potential well width at the Fermi energy). Hence, the effect of the real dopant distribution on the subband positions is only marginal for the samples investigated and the model of Reisinger

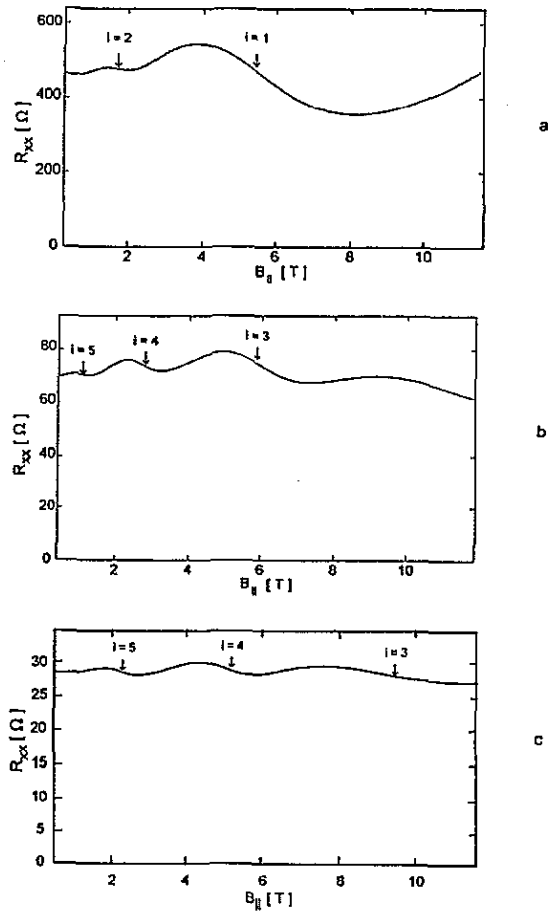

Figure 6. Diamagnetic SdH effect of the samples sδ-2364 (*a*), sδ-2329 (*b*) and sδ-2330 (*c*). The depopulation fields of the corresponding subbands (index *i*) are marked by arrows.

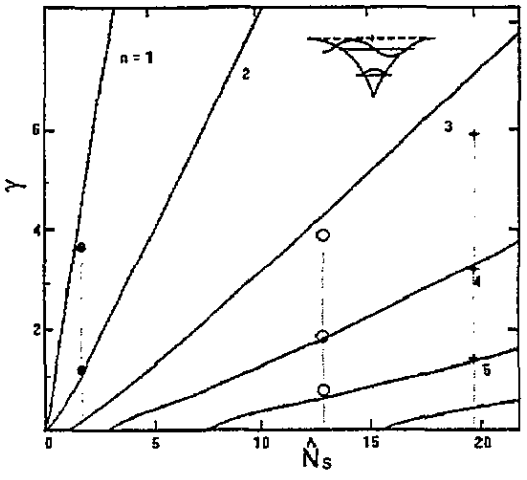

Figure 7. Comparison of the normalized depopulation fields γ of the diamagnetically shifted subbands of samples sδ-2364 (●), sδ-2329 (○) and sδ-2330 (+) with the dependences on the normalized carrier density $\tilde{N}_s$ obtained by Reisinger and Koch [10] for symmetrical potential wells (full lines). The inset shows schematically the potential well, the first two subband levels and the corresponding wave functions.

and Koch [10] provides a satisfactory description of our experimental results. If the depopulation fields of the subbands are plotted versus the carrier concentration in dimensionless units of

$$\gamma = (\hbar\omega_c/e^2)4\pi\epsilon a^* = (2h^3\epsilon^2/\pi e^3 m^{*2})B \qquad (2)$$

where a^* is the effective Bohr radius, h is Planck's constant, ω_c is the cyclotron frequency, m^* is the effective electron mass and

$$\bar{N}_s = n_s a^{*2} = (h^4\epsilon^2/\pi^2 e^4 m^{*2}) n_s \tag{3}$$

the influence of the material properties and the band structure (ϵ and m^*) on the depopulation behaviour is (at least partially) eliminated and 'universal' dependences appear [10]. As visible in figure 7, the depopulation fields of our differently doped samples are well described within this model of Reisinger and Koch [10] for symmetrical potential wells.

4. Summary

We have performed galvanomagnetic measurements on MBE-grown silicon δ-doped $Ga_{0.47}In_{0.53}As$ layers to determine the Hall mobility, the total sheet electron density and the subband populations. Samples with a varying doping level and corresponding sheet densities ranging from $n_s = 8.2\times10^{11}$ cm^{-2} to 9.3×10^{12} cm^{-2} were investigated.

Several electric subbands were found to be populated in all samples. The depopulation of the higher subbands by parallel magnetic fields is visible in the DSdH spectra of the samples and can be explained within the Reisinger–Koch model for symmetrical potential wells.

In the sample with the lowest electron density, all electrons are redistributed into the lowest subband for parallel magnetic fields in excess of 5.6 T. This leads to a well pronounced QHE in tilted magnetic fields, whereas magnetic fields up to 12 T perpendicular to the δ-doping layer were not sufficient to form QH plateaux. Hence, the diagmagnetic depopulation of the higher subbands by the parallel magnetic field component is essential in observing the QHE in silicon δ-doped $Ga_{0.47}In_{0.53}As$ layers with several subbands populated.

Acknowledgments

We would like to thank Dr H G Bach for fruitful discussions and J Böttcher for expert help with the MBE growth.

References

[1] Wood C E C, Metze G, Berry J and Eastman L F 1980 *J. Appl. Phys.* **51** 383
[2] Döhler G H 1978 *Surf. Sci.* **73** 97
[3] Koch F and Zrenner A 1989 *Mater. Sci. Eng.* B **1** 221
[4] Zrenner A, Reisinger H, Koch F, Ploog K and Maan J C 1986 *Phys. Rev.* B **33** 5607
[5] Zrenner A 1989 *Appl. Phys. Lett.* **55** 156
[6] Ye Qiu-Yi, Zrenner A, Koch F and Ploog K 1989 *Semicond. Sci. Technol.* **4** 500
[7] Hong W-P., DeRosa F, Bhat R, Allen S J and Hayes J R 1989 *Appl. Phys. Lett.* **54** 457
[8] diForte-Poisson M A, Brylinski C, Favre J, Ranz E, Lavielle D and Portal J C 1992 *Proc. 4th Int. Conf. on InP and Related Materials, Newport/USA* (IEEE Catalog No 92CH3104/7) p 163
[9] Passenberg W, Bach H G and Böttcher J 1991 *J. Electron. Mater.* **20** 989
[10] Reisinger H and Koch F 1986 *Surf. Sci.* **170** 397
[11] Nachtwei G, Bassom N J, Nicholas R J, Preppernau U and Herrmann R 1989 *Semicond. Sci. Technol.* **4** 747
[12] Nachtwei G, Schulze D, Gobsch G, Paasch G, Kraak W, Krüger H and Herrmann R 1988 *Phys. Status Solidi* b **148** 349
[13] Gobsch G, Schurig Th, Kraak W, Herrmann R and Pasch G 1989 *J. Physique* **50** 283